Eur. Phys. J. B **5**, 847–858 (1998)

THE EUROPEAN PHYSICAL JOURNAL B

Low temperature penetration depth and the effect of quasi-particle scattering measured by millimeter wave transmission in $YBa_2Cu_3O_{7-\delta}$ thin films

S. Djordjevic[1], L.A. de Vaulchier[1,a], N. Bontemps[1], J.P. Vieren[1], Y. Guldner[1], S. Moffat[2], J. Preston[2], X. Castel[3], M. Guilloux-Viry[3], and A. Perrin[3]

[1] Laboratoire de Physique de la Matière Condensée, École Normale Supérieure, 24 rue Lhomond, 75231 Paris Cedex 05, France
[2] Brockhouse Institute for Materials Research, McMaster University, Hamilton On. L8S 4M1, Canada
[3] Laboratoire de Chimie du Solide et Inorganique Moléculaire, Université de Rennes I, avenue du Général Leclerc, 35042 Rennes Cedex, France

Received: 22 January 1998 / Revised: 18 May 1998 / Accepted: 9 June 1998

Abstract. Measurement of the penetration depth $\lambda(T)$ as a function of temperature using millimeter wave transmission in the range 130–500 GHz are reported for three $YBa_2Cu_3O_{7-\delta}$ (YBCO) laser ablated thin films. Two films, deposited on a $LaAlO_3$ substrate ($T_c = 90.2$ K), exhibit a narrow resistive transition (0.3 K). One has been subsequently irradiated with He^+ ions in order to increase the scattering rate of the quasi-particles ($T_c = 87.8$ K). The third film, grown on MgO ($T_c = 88.5$ K), exhibits also a fairly narrow transition (0.8 K) and a high crystalline quality. The experiment provides the absolute value $\lambda(T \leq 30\,\mathrm{K})$ for the penetration depth at low temperature: the derivation from the transmission data and the experimental uncertainty are discussed. We find a zero temperature penetration depth $\tilde{\lambda_0} = 1990 \pm 200$ Å, 2180 ± 200 Å and 2180 ± 200 Å, for YBCO-500 Å/$LaAlO_3$ (pristine), YBCO-1300 Å/MgO and YBCO-500 Å/$LaAlO_3$ (irradiated) respectively. $\lambda(T \leq 30\,\mathrm{K})$ exhibits a different behavior for the three films. In the pristine sample, $\lambda(T \leq 30\,\mathrm{K})$ shows a clear *temperature and frequency dependence*, namely the temperature dependence is consistent with a linear variation, whose slope decreases with frequency: this is considered as an evidence for the scattering rate being of the order of the measuring frequency. A two fluids analysis yields $1/\tau(T \leq 30\,\mathrm{K}) \sim 1.7 \times 10^{12}\,\mathrm{s}^{-1}$. In the two other samples, $\lambda(T \leq 30\,\mathrm{K})$ does not display any frequency dependence, suggesting a significantly larger scattering rate. The temperature dependence is different in these latter samples. It is consistent with a linear variation for the YBCO/MgO sample, not for the YBCO/$LaAlO_3$ irradiated one, which exhibits a T^2 dependence up to 40 K. We have compared our data to the predictions of the *d*-wave model incorporating resonant scattering and we do not find a satisfactory agreement. However, the large value of $\tilde{\lambda_0}$ in the pristine sample is a puzzle and sheds some doubt on a straightforward comparison with the theory of data from thin films, if considered as dirty *d*-wave superconductors.

PACS. 07.57.c Infrared, submillimeter wave, microwave and radiowave instruments, equipment and techniques – 74.72.h High-T_c compounds – 74.76.w Superconducting films

1 Introduction

The study of the in-plane penetration depth $\lambda(T)$ and its temperature dependence has been widely investigated since the discovery of high-T_c cuprates. Being directly related to the superfluid density, it probes the density of excited quasi-particles (QP), and therefore it is closely related to the symmetry of the gap. One of the key experiment in favor of an unconventional order parameter with lines of nodes was the evidence of a linear temperature dependence of $\lambda(T)$ in YBCO single crystals [1]. Such a linear dependence has been now observed in a variety of cuprates, *e.g.* $Bi_2Sr_2CaCu_2O_{8+\delta}$, $Tl_2Ba_2CuO_{6+\delta}$ and $Hg_2Ba_2Ca_{n-1}Cu_nO_{2n+2+2\delta}$, [2–5] with slopes ranging from 4 to 13 Å K^{-1}. This behavior is consistent with a $d_{x^2-y^2}$ order parameter which is presently strongly in favor, supported by photoemission [6] and phase sensitive data in $Bi_2Sr_2CaCu_2O_{8+\delta}$, YBCO, $Tl_2Ba_2CuO_{6+\delta}$ [7]. However, the precise symmetry of the order parameter is still controversial or may differ in the various cuprate families, in particular in YBCO, $Bi_2Sr_2CaCu_2O_{8+\delta}$ or $La_{2-x}Sr_xCu_{4+\delta}$ [8–10]. In YBCO, suggestions have been brought up from experiments, including the admixture of a significant *s*-wave component [7] and the claim for a two-components

[a] e-mail: Louis-Anne.deVaulchier@physique.ens.fr

order parameter [11]. Going beyond qualitative tests of the symmetry is difficult. It requires a model providing quantitative predictions. Such models have been developed. We mention here some of them, namely pure $d_{x^2-y^2}$ order parameter in the framework of the spin fluctuations theory [12], $s+d$ symmetry related to YBCO orthorhombic structure [8], anisotropic s-wave [9] or *plane-chain coupling* in YBCO [13]. There is a large body of literature which discusses in detail the microwave behavior of a d-wave superconductor in the presence of scattering. We briefly recall those features of the model which deal with the penetration depth and the high frequency conductivity. The change of (i) the critical temperature T_c, (ii) the superfluid density at zero temperature $\rho_s \propto 1/\tilde{\lambda_0^2}$ where $\tilde{\lambda_0}$ is the zero temperature penetration depth, (iii) the temperature dependence of $\lambda(T)$, has been calculated as a function of the impurity concentration and/or the scattering rate in the unitary limit [14–17]. This latter limit may explain why a very small amount of impurities or defects responsible for elastic scattering, while hardly affecting the critical temperature, strongly modifies the superfluid density, hence the penetration depth and its temperature dependence. Two regimes are expected to develop successively: the first one (the so-called gapless regime) holds from low temperature up to a crossover temperature T^*, and the temperature dependence of $\lambda(T)$ is T^2. The second one is the clean regime where the linear temperature dependence is recovered [15–17].

Presently, it seems clearly settled that the low temperature dependence of $\lambda(T)$ in YBCO single crystals (*taken henceforward as examples of the clean system*) is linear up to $\sim 30\,\mathrm{K}$ with a slope of 4 to 5 Å K^{-1} [1,18,19]. Thin films have been considered as possible examples of "dirty" samples, although there is evidence for a linear temperature dependence with a slope similar to that of crystals [20–22]. Deviations from this linear regime is however commonly reported in thin films, whether the linear dependence does not display the "canonical" slope [23–25] or the dependence is rather T^2 [26–30]. The latter behavior has been argued to arise from defects likely to be present in thin films and playing the role of impurities in the unitary limit. A quantitative comparison to the d-wave model was claimed to apply successfully to such samples [26,27]. A similar comparison has been performed in purposely impurity-doped YBCO single crystals [31]. Note that the experimental techniques used in the above mentioned reports provide the change of $\lambda(T)$ with temperature, but not its absolute value with a sufficient accuracy. The single crystal data have been analyzed by Hirschfeld *et al.* within the framework of the d-wave model [17]. The conclusion was that, as long as the absolute value $\tilde{\lambda_0}$ was not known, "roughly equally good fits" may be obtained with various scattering rates, the latter being consistent or not with the initial assumption of the scattering rate scaling with the impurity concentration. Some of the thin film data did not display a satisfactory agreement with d-wave theory either [32]. Similar restrictions were also raised by Hensen *et al.* when analyzing their own thin film data [24].

We report in this paper penetration depth results obtained in three selected thin films (which we describe specifically in Sect. 4). The penetration depth is deduced from far infra red (FIR) transmission of an electromagnetic wave through the sample, one technique among very few others which yields not only the variation of $\lambda(T)$ with temperature, but its zero temperature value $\tilde{\lambda_0}$ [20,33,34]. As already stated, this is a key parameter for a reliable comparison with theoretical models. Moreover, the experiment being performed between 130 and 510 GHz, at several frequencies (usually 5), the corresponding time scale becomes comparable to the low temperature QP scattering time τ (typically, 300 GHz corresponds to $1/\tau \sim 2\times 10^{12}\,\mathrm{s}^{-1}$). This manifests itself through a dependence of the measured penetration depth as a function of frequency and can be analyzed quantitatively in the frame work of a generalized two fluids model including a Drude conductivity for the normal fluid [23, 31,35–37]. We demonstrate that our data display a satisfactory agreement with this phenomenology and extract the low temperature ($T \leq 30\,\mathrm{K}$) elastic scattering rate. This is in contrast with earlier work where the internal consistency of the two fluids model could not be checked since the measurements were performed as a function of temperature, at one or two frequencies. Therefore a two fluids conductivity had to be assumed in order to deduce the scattering rate either from surface resistance data in single crystals [36] or from FIR or THz spectroscopy in presumably good quality films [37–39]. Since our experiment yields $\tilde{\lambda_0}$ and $\lambda(T)$, we derive from this set of data three parameters of the model, namely $\delta\lambda_0 = \tilde{\lambda_0} - \lambda_0$ (λ_0 is the penetration depth of the clean system), T^* and T_c/T_{c0} (T_c and T_{c0} are the actual transition temperature and the one of the clean system respectively). We shall take T_c at zero resistance (Tab. 1) and $T_{c0} = 92\,\mathrm{K}$. We then compare to the values these parameters should achieve in the case of the d-wave model in presence of resonant scattering. As will be shown, the model clearly fails to account for the data in all the films under investigation in this paper. Since more experimental parameters are available from our experiment than from the others, our results shed some doubt on the previous claims that thin films can be properly described in the framework of the d-wave model by simply incorporating resonant scattering.

Our paper proceeds as follows: in Section 2, we describe the experimental setup. Section 3 describes in detail the data processing from which the absolute value of the penetration depth $\tilde{\lambda_0}$ and its temperature variation are derived, and introduces the frequency dependent penetration depth $\lambda(\omega, T)$. The samples are described in Section 4. Section 5 summarizes the penetration depth data. In Section 6 we recall the so-called generalized two fluids model, and stress the consequences on the variation of $\lambda(\omega, T)$ when the low temperature QP scattering rate $1/\tau$ becomes comparable to the measuring frequency ω. This leads us to an estimate of $1/\tau$. Section 7 is devoted to a comparison of our experimental data with

Table 1. Characteristics of the three samples MA, MB and LR: prep. (growth technique), critical temperature T_c and resistive width ΔT_c, thickness d of the film, thickness l of the substrate, width $\Delta\theta$ of the rocking curve (when available), surface resistance R_S at 10 GHz and 77 K (when available), irradiation dose by He ions.

Sample	prep.	$T_c(R=0)$ (K)	ΔT_c (K)	d (Å)	$\rho_{110\,\mathrm{K}}$ ($\mu\Omega$cm)	l (μm)	$\Delta\theta$	R_S (mΩ)	He (10^{14} He/cm^2)
MA	laser	90.2	0.3	500	90	515			none
MB	laser	89.7	0.3	500	80	510			none
	after irr.	87.8	0.6		105				2
LR	laser	88.5	0.8	1300	100	515	0.23°	2	none

the d-wave model, assuming that thin films may be examples of d-wave superconductors, however including strong scattering due to their specific defects.

2 Experimental

We briefly recall the general features of the experimental millimeter transmission setup that has been described in detail elsewhere [20,33,40] and point out some late modifications. The sources are carcinotrons operating typically at 134, 250, 333, 387 and 510 GHz. The 510 GHz source can be tuned in a typical 50 GHz range. At 387 GHz, tuning is possible but difficult. These sources deliver from 1 to 300 mW and are very stable (± 0.1 dB per hour). A continuously tunable 110–180 GHz backward wave oscillator (BWO) is also available, which provides an output power of typically 5 mW and a stability of ± 0.3 dB. The radiation is guided through oversized (10 mm diameter) circular wave guides, which allow us to change the frequency, onto the sample placed in a helium flow cryostat. The sample is tightly fixed with silver paste (to avoid leakage) on a brass sample holder (with a 3 mm or 4 mm iris) and is surrounded by a helium exchange gas (100 mbar pressure at room temperature) to damp out temperature instabilities in the helium flow at our lowest temperatures. The transmitted signal is detected by a He cooled InSb bolometer with a 60 dB linearity range. We have checked that the microwave leakage represents more than 60 dB attenuation. Samples are screened from stray magnetic field, so that the residual magnetic field is less than 0.5 Oe. The main limitation to the accuracy of this experiment is associated with the multi-mode propagation within the oversized guides, giving rise to a set of standing waves which are subject to thermal drifts (this problem, discussed in some detail below, has been carefully analyzed using the tunable BWO). To minimize those thermal drifts, the guides within the cryostat are made out of invar, and are as short as possible, compatible with a good temperature stability of the sample holder (± 0.2 K). The measurements are performed by slowly varying the temperature from 6 K to 110 K, at fixed frequency.

3 Data processing

3.1 Transmission of a thin film

For the sake of emphasizing the physics of the measurement, we firstly neglect in this paragraph the interference pattern due to the substrate. We consider a film of thickness d (smaller than the wavelength of the electromagnetic wave, the skin depth in the normal state or the penetration depth in the superconducting state) deposited on a substrate of index n. The transmission with respect to the one of the substrate reads [41]:

$$T_r(\omega,T) = \frac{1}{\left|1+\dfrac{\sigma(\omega,T)dZ_0}{1+n}\right|^2} \tag{1}$$

where $Z_0 = 377\ \Omega$ is the impedance of the free space. $\sigma(\omega,T) = \sigma_1(\omega,T) - i\,\sigma_2(\omega,T)$ is the complex conductivity of the film, and $Z(\omega,T) = 1/\sigma(\omega,T)d$ is the impedance of the film. The imaginary part of the conductivity writes:

$$\sigma_2(\omega,T) = \frac{1}{\mu_0\omega\lambda_L^2(T)} \tag{2}$$

where $\lambda_L(T)$ is the London penetration depth [42]. The usual condition for this expression of $\sigma_2(\omega,T)$ to be valid is that the working frequency must lie far below the superconducting (isotropic) gap Δ ($\omega \ll 2\Delta$) [42]. In cuprates in general, and YBCO in particular, experiments including the penetration depth data show that the gap exhibits nodes in some directions of the k space. Therefore the condition $\omega \ll 2\Delta(k)$ is not fulfilled in all directions of the k space. Nevertheless, the density of states at finite energy ω is expected to be small compared to that at the maximum gap energy Δ_m [43], as long as $\omega \ll 2\Delta_m$. In this case, we consider that the electromagnetic response is dominated by the one of the superfluid, and that the contribution from QP generated through pair-breaking by the EM wave is negligible. Our highest frequency (17 cm^{-1}) is now to be compared to $2\Delta_m$. Tunneling data locate a maximum around 25 meV [44]. If this feature is assigned to the maximum gap, then indeed $\omega \ll 2\Delta_m = 400$ cm^{-1}.

In order now to deduce $\lambda_L(T)$ from (1), another condition is that $\sigma_2(\omega,T)$, as given above, be much larger than $\sigma_1(\omega,T)$, which is well-known at low temperature for a BCS-type superconductor. In an unconventional superconductor with nodes in the gap, the conductivity may involve a contribution arising from thermally excited QP [16,17,24]. The real part of the conductivity for a *d*-wave superconductor, in the presence of inelastic as well as elastic scattering, exhibits a Drude-like expression, however including now a frequency-dependent QP scattering rate [16,17,24]. As further discussed below, these approaches have not proven completely successful in order to account for the experimental data. In the following, we shall use two different frameworks for data analysis: (i) as many other authors, a generalized two fluids conductivity, where the QP scattering rate does not depend upon the frequency, in order to account for the presence of unpaired carriers; (ii) the *d*-wave model for the conductivity in presence of elastic scattering due to impurities or defects [14–17].

At this stage, we define the conductivity, by including a real part $\sigma_1(\omega,T)$ arising from the normal fluid and an imaginary part $\sigma_2(\omega,T)$ where the contribution of the normal fluid is included formally in a frequency and temperature dependent penetration depth $\lambda(\omega,T)$:

$$\sigma(\omega,T)=\sigma_1(\omega,T)-\frac{1}{\mu_0\omega\lambda^2(\omega,T)}. \tag{3}$$

The dependence of the generalized penetration depth $\lambda(\omega,T)$ on the frequency depends, as will be shown further, on the relative value of the frequency and the QP scattering rate $1/\tau$. In the quasi-static regime, *e.g.* at very low frequency ($\omega\tau \ll 1$), the generalized penetration depth does not depend on the frequency. In this limit $\lambda(\omega,T)$ may be identified to the London penetration depth $\lambda_L(T)$ [18,33,45]. The conductivity defined in (3) is then plugged in the transmission (1), and the absolute value of the penetration depth and its temperature dependence may then be deduced as explained in Sections 3.2 to 3.4. Note that we have checked the temperature independence of the index n of the substrate in our frequency range [33].

3.2 Normalized transmission and the basics of penetration depth measurements

Equation (1) involving the complex conductivity depends upon two quantities, $\sigma_1(\omega,T)$ and $\sigma_2(\omega,T)$, and only a single measurement is available. However, we are interested in the low temperature behavior of the transmission. In a BCS superconductor, one has $\sigma_2(\omega,T) \gg \sigma_1(\omega,T)$ (actually even close to T_c). In this case, the transmission depends only on $\sigma_2(\omega,T)$, hence on $\lambda(\omega,T)$. In high-T_c superconductors, the question is less simple: it is known from experiments that $\sigma_1(\omega,T)$ *increases* below T_c, exhibits a maximum around 40 K at frequencies ≤ 50 GHz [23,25,35,36], which shifts toward higher temperature at higher frequency (typically 60 K at 300 GHz as measured in thin films [24,38,39]). It is therefore not obvious that $\sigma_1(\omega,T)$ is negligible with respect to $\sigma_2(\omega,T)$ in our frequency range. All data in the literature show however that, at low temperature, *e.g.* below 30 K, which is the range of interest in the present paper, the approximation $\sigma_1(\omega,T) \ll \sigma_2(\omega,T)$ holds [18,23–25,35,36,38,39] hence $T_r(\omega,T)$ is eventually simply related to the penetration depth.

The absolute value of the transmission, $T_r(\omega,T)$ cannot be determined in our setup. Such an absolute measurement is possible in a setup which allows quasi-optical propagation [30,46]. However, in our case, replacing the sample by a hole or a bare substrate changes the standing waves within the guides, thus biasing the measurement of the reference incident power. In order to circumvent the difficulty, we choose to normalize the transmission with respect to the one in the normal state at 110 K:

$$\frac{T_r(\omega,T)}{T_r(110\,\mathrm{K})}=\frac{\left(1+\frac{\sigma(110\,\mathrm{K})\,dZ_0}{1+n}\right)^2}{1+\left(\frac{dZ_0}{(1+n)\mu_0\omega\lambda^2(\omega,T)}\right)^2} \tag{4}$$

which will be henceforward referred to as the normalized transmission T_n. The normalization makes sense (*e.g.* the normalized transmission yielding the penetration depth value as shown in (4)) only if the transmission is independent of the frequency in the normal state at 110 K. This turns out to be right in our frequency range: considering the value of the scattering rate $1/\tau \sim 2\times10^{13}\,\mathrm{s}^{-1}$ in the normal state (at $T \geq T_c$) inferred from surface impedance data [31,35,36], the condition $\omega\tau \ll 1$ is verified and the conductivity is frequency independent. Finally, the choice of 110 K is a compromise for a temperature high enough above T_c so as to avoid conductivity fluctuations which may be frequency dependent (but are still negligible at 110 K) and low enough in order to minimize the thermal drifts due to thermal expansions of the guides (which are negligible at 110 K).

3.3 Interference pattern, derivation of $\tilde{\lambda_0}$ and $\lambda(\omega,T)$

Equation (4) does not account for the interference fringes due to the substrate. In experiments using quasi-optical techniques, the interference pattern is very well identified [30,37,46]. From the calculation of this pattern in the case of a plane wave [41], we know that the contrast of the fringes increases considerably with frequency: it is 10 times larger at 500 GHz than at 130 GHz (Fig. 1). Therefore, we expect an interference effect to be more conspicuous at our largest frequency. Since we have no broadly tunable source in the range 300–500 GHz, we cannot measure directly this pattern. Moreover, in our setup, due to the multimode propagation, it is not clear to which extent this pattern may be modified. We therefore compare the transmission data to the theoretical transmission including the interference effect, in the simple case of a plane wave. If the interference effect were negligible, the data should follow the simplified transmission resulting from (4).

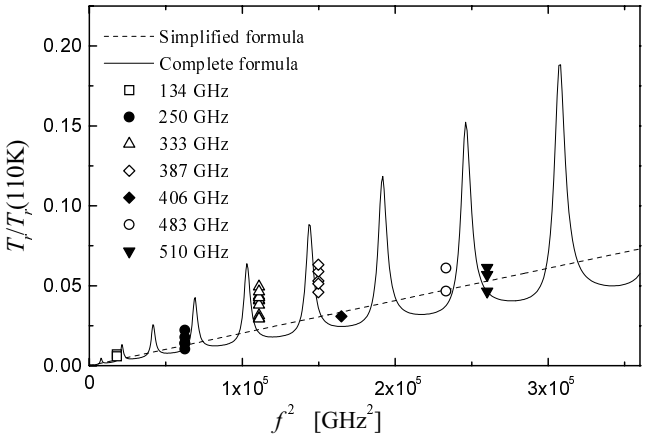

Fig. 1. Normalized transmission $T_{10\,\mathrm{K}}/T_{110\,\mathrm{K}}$ *versus* the square of the frequency in sample MA. For a same nominal frequency, each point corresponds to an experimental run, after which the sample is dismounted before running the measurement again. The interference pattern (solid line) is calculated [41] using $l = 515\,\mu$m, $n = 5$ and $\lambda(10\,\mathrm{K}) = 2000$ Å in order to fit the experimental data. The dashed line represents (4), *e.g.* the simple expression for the normalized transmission, neglecting the interference pattern, for the same parameters n and $\lambda(10\,\mathrm{K})$.

Figure 1 displays a set of normalized transmission data from sample MA for the various frequencies $f = \omega/2\pi$ ranging from 130 to 510 GHz, as a function of f^2, at 10 K (although the penetration depth data will be reported in the range 6 K–110 K, we have collected many more data starting from 10 K). Clearly, despite the experimental scatter, one cannot fit the whole set of data with a straight line (Eq. (4)), due to the highest frequency data. This strongly suggests that the interference effect must be taken into account.

Let us comment firstly about the experimental scatter. The experimental points at each frequency correspond to different sets of experimental runs, *e.g.* the sample has been removed then put back into the cryostat. This affects the standing waves by changing the boundary conditions. We have established, after a detailed study, that this scatter is due to thermal drifts occurring above 40 K as the temperature is swept from 6 K to 110 K. This obviously affects the normalized transmission since the normalization is performed with respect to the 110 K transmission. Figure 1 shows the best fit of our data with a given pattern. The agreement is obtained by adjusting the value of the penetration depth and of the thickness l of the substrate. We find: $\lambda(\omega, 10\,\mathrm{K}) = 2000 \pm 100$ Å (the frequency dependence is neglected, this assumption being reasonable at low enough temperature [16,17,45]) and $l = 515 \pm 10\,\mu$m, the nominal thickness being 500 μm. The uncertainty on the penetration depth arises mainly from the scatter of the experimental points. To assert this fit, the value of the thickness l of the substrate was: (i) double checked by a direct measurement (also within $\pm$ 10 μm) with a micrometer screw, (ii) compared with the value obtained from the fringe pattern observed in a transmission measurement performed at LURE using far infrared synchrotron radiation in the range 20−45 cm^{-1} (yielding the optical path $2nl$), combined with an infrared measurement of n [47,48].

Obviously, we do not use this fitting procedure to establish the value of $\lambda(\omega, T)$ at each temperature, since its variation up to 30 K is expected to be small compared to the uncertainty (taking the "canonical" value of 4 Å K^{-1} from single crystals). We can however derive with a much better accuracy the relative change of $\lambda(\omega, T)$ as a function of temperature, starting from 6 K, since there are no thermal drifts in this temperature range. We proceed as follows. Given the best fit at 10 K (Fig. 1), a factor $\beta_0(f)$ for each experimental frequency f defines the correspondence between the actual data (including the interference effect) and the simplified expression for the normalized transmission neglecting the interference effect (satisfying Eq. (4)). We multiply the temperature dependent normalized transmission by $\beta_0(f)$ and then we deduce $\lambda(\omega, T)$. $\beta_0(f)$ itself is in principle temperature dependent, but we have checked that this temperature dependence (which we may write to first order as $\beta(T) = \beta_0 + \beta_1 T$) is negligible. We have estimated $\beta_1 \sim 10^{-3}\beta_0\,\mathrm{K}^{-1}$. This also implies that the choice of the reference temperature where the correction factor is established is unimportant. Finally, the absolute value $\tilde{\lambda_0}$ is determined by extrapolation to zero temperature of $\lambda(\omega, T)$.

3.4 Estimate of the experimental uncertainty on $\tilde{\lambda_0}$

The uncertainty on $\tilde{\lambda_0}$ comes firstly from the experimental scatter (Fig. 1). From the set of different experiments, we have observed a scatter of the normalized transmission of the order $\pm$ 40% at 134 and 250 GHz and $\pm$ 25% at 510 GHz. This results roughly in a scatter of $\pm$ 10% for the penetration depth, hence $\pm$ 200 Å for a typical value of 2000 Å. This uncertainty incorporates the error of $\pm$ 100 Å which we mentioned in the fitting to the interference pattern.

A second type of uncertainty is a systematic error due to the value of the resistivity $\rho_{110\,\mathrm{K}}$ at 110 K, needed in the calculation of the penetration depth. According to our own measurements (using the Van Der Pauw technique) or other 4 points measurements requiring a different geometrical factor, we estimate the error on $\rho_{110\,\mathrm{K}}$ to $\pm$ 10% which typically leads to $\pm$ 5% on the penetration depth since it scales like $\rho_{110\,\mathrm{K}}^{1/2}$. For 2000 Å, it represents $\pm$ 100 Å. This error is different from sample to sample, but it is a systematic one. Moreover, it is smaller than the $\pm$ 200 Å experimental uncertainty due to thermal drifts. Finally, the absolute value $\tilde{\lambda_0}$ results from an extrapolation at zero temperature. According to the temperature variation which is observed, such an extrapolation cannot generate an error larger than 40 Å. The absolute values for the penetration depth will therefore be given within $\pm$ 200 Å.

4 Samples

We present the results which we have obtained on three epitaxially grown, laser ablated good quality YBCO thin films (referred as sample MA, MB, and LR). Samples MA and MB are deposited on $LaAlO_3$, and LR on MgO. The substrates have a nominal 500 μm thickness and through fitting, the thickness is found close to 510 μm. The characteristics of the samples are shown in Table 1.

The growth conditions of MA and MB samples have been described elsewhere [49]. The thickness of the films was not measured, but is estimated to be 500 Å, based on measurements in similar samples which had been patterned by photolithography. Not knowing precisely the thickness is not a serious problem since it enters only as a correction in the analysis of the transmission. Both samples display a resistivity varying linearly with temperature, with close to zero extrapolation, and a narrow transition (0.3 K). These widths are indicative of good quality samples, although the transition temperatures could be higher for samples deposited onto $LaAlO_3$. Sample MB was then irradiated in order to introduce point defects, following the conditions reported in a systematic study of ion irradiated YBCO films [49]. After irradiation, the resistive transition of sample MB is lowered by 1.9 K and slightly broadened (0.6 K).

Sample LR was grown by laser ablation according to the method explained in [50,51]. It has a narrow transition (0.8 K), its critical temperature is lower than the one obtained in samples grown on $LaAlO_3$ as usually observed for films grown on MgO. The narrow rocking curve ($\Delta\theta = 0.23°$) is indicative of a good c-axis orientation. Films grown on MgO often display simultaneous in-plane epitaxial growth along the [100] and [1$\bar{1}$0] directions, which is very detrimental to surface resistance hence, as was shown earlier, to the penetration depth [50]. This specific sample was selected for its weak admixture of [1$\bar{1}$0] grains (5%), giving rise to $R_S(10\,\mathrm{GHz}, 77\,\mathrm{K}) \simeq 2\,\mathrm{m\Omega}$, deduced from the experimental correlation between low frequency and microwave frequency losses [51]. This value is still much larger than what is now commonly obtained in YBCO films, *e.g.* $R_S(10\,\mathrm{GHz}, 77\,\mathrm{K}) \leq 0.5\,\mathrm{m\Omega}$.

5 Penetration depth results

We report now the penetration depth data derived as explained in the previous section for the 3 samples examined in this paper. Figure 2 displays the results for sample MA (non irradiated, $LaAlO_3$). We have plotted the penetration depth for $6\,\mathrm{K} \leq T \leq 60\,\mathrm{K}$ at five frequencies: 134, 250, 333, 387 and 510 GHz.

The first parameter we extract is the value $\tilde{\lambda_0} = 1990 \pm 200$ Å for this sample, to be compared to the values found in single crystals: 1450 Å, from muon spin rotation [52] or 1300 Å (an average of the penetration depth along the a and b directions measured by infrared reflectivity [53]), these values being believed to be close to the intrinsic value. Figures 3 and 4 display the low temperature behavior, $6\,\mathrm{K} \leq T \leq 30\,\mathrm{K}$, which is the one we focus on in this study for the sake of the comparison to YBCO single crystals, where the linear temperature dependence holds up to 30 K. Figure 3 is a plot *versus* T and Figure 4 *versus* T^2. The data have been systematically shifted by 20 Å for clarity, starting from the highest frequency. Whichever plot is considered, one notices immediately that the temperature dependence of the penetration depth $\lambda(\omega, T)$ becomes less and less pronounced as the frequency increases. In this temperature range, we assign this behavior to the frequency becoming

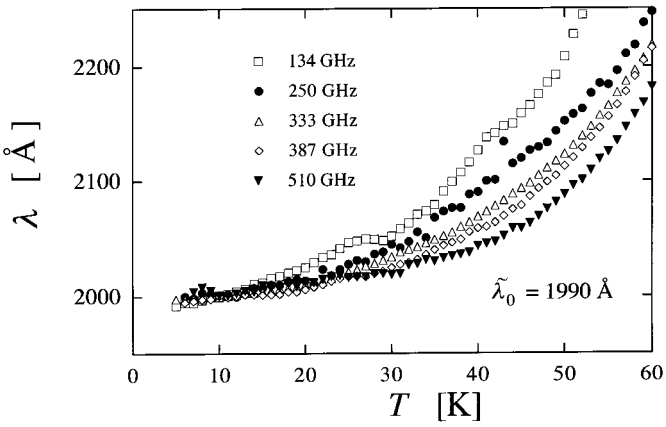

Fig. 2. Penetration depth for sample MA *versus* temperature for $T \leq 60\,\mathrm{K}$ at various frequencies: 134, 250, 333, 387, 510 GHz. Above 60 K, the derivation of $\lambda(\omega, T)$ is no longer valid. $\tilde{\lambda_0}$(extrapolated) = 1990 Å. The frequency dependence of the penetration depth below $T \leq 30\,\mathrm{K}$ is clearly amplified above this temperature.

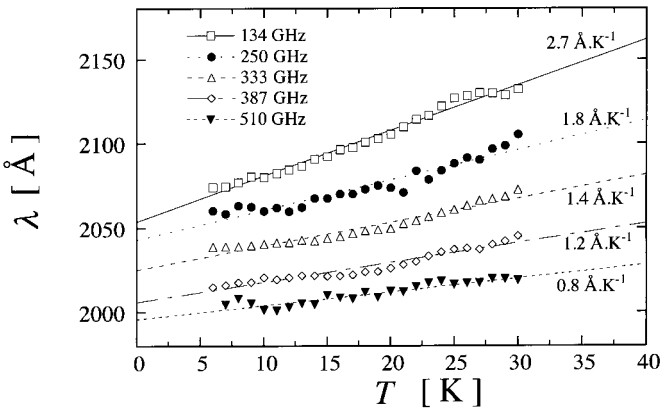

Fig. 3. Penetration depth for sample MA *versus* temperature T for $T \leq 30\,\mathrm{K}$ (where a linear regime is commonly observed in single crystals) for five frequencies: 134, 250, 333, 387, 510 GHz. Best fits to a linear variation $\lambda(\omega, T) = \tilde{\lambda_0} + c_1(\omega)\,T$ are displayed for each curve as well as the value $c_1(\omega)$ of the slope. The curves are systematically shifted up by 20 Å for clarity, starting from the highest frequency. This figure shows clearly the change of the temperature dependence with increasing frequency.

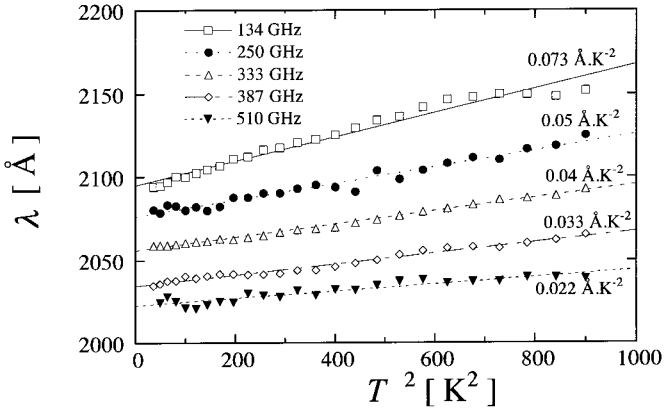

Fig. 4. Same data as in Figure 3 plotted *versus* T^2. Best fits to a T^2 variation $\lambda(\omega,T) = \tilde{\lambda_0} + c_2(\omega)\,T^2$ are displayed for each curve, as well as the value of $c_2(\omega)$. Within the accuracy of the measurement, we cannot really distinguish between a T or T^2 dependence.

Table 2. $c_1(\omega)$ and $c_2(\omega)$ for samples MA and LR at the various frequencies. The parameters $c_1(\omega)$ and $c_2(\omega)$ are defined through the fitting of the penetration depth (shown in Figs. 3, 4, 6 and 7) to $\lambda(\omega,T) = \tilde{\lambda_0} + c_1(\omega)\,T$ and $\lambda(\omega,T) = \tilde{\lambda_0} + c_2(\omega)\,T^2$ respectively. The uncertainty is $\pm$ 0.7 Å K^{-1} on $c_1(\omega)$ and $\pm$ 0.03 Å K^{-2} on $c_2(\omega)$.

	Sample MA		**Sample LR**	
Frequency	$c_{1\,exp}(\omega)$	$c_{2\,exp}(\omega)$	$c_{1\,exp}(\omega)$	$c_{2\,exp}(\omega)$
(GHz)	(Å K^{-1})	(Å K^{-2})	(Å K^{-1})	(Å K^{-2})
134	2.7	0.073	3.1	0.086
250	1.8	0.050	3.3	0.096
333	1.4	0.040	1.6	0.043
387	1.2	0.033	2.2	0.054
510	0.8	0.022	2.0	0.058

comparable to the scattering rate ($\omega\tau \sim 1$) [16–18,45]. A similar qualitative change of the temperature dependence of $\lambda(\omega,T)$ has been reported using two frequencies: 18.9 GHz (cavity resonator technique) and 300 GHz (quasi-optical interferometer) [37]. Our study has the advantage to use a single technique and five frequencies, therefore allowing a more detailed analysis of the frequency effect on $\lambda(\omega,T)$, as discussed below.

It is not possible to decide whether the temperature dependence is linear or quadratic. The data are not accurate enough, but in any case, as pointed out by Hirschfeld *et al.* [16,17], once the temperature variation of the penetration depth is observed to be frequency dependent, there is no analytic fit which would apply for all frequencies. We have nevertheless quantified the effect of the frequency on the penetration depth assuming either $\lambda(\omega,T) = \tilde{\lambda_0} + c_1(\omega)\,T$ (Fig. 3) or $\lambda(\omega,T) = \tilde{\lambda_0} + c_2(\omega)\,T^2$ (Fig. 4). The value of the fitted parameters $c_1(\omega)$ and $c_2(\omega)$ are reported in Table 2, within an error bar of $\pm$ 0.7 Å K^{-1} and $\pm$ 0.03 Å K^{-2}.

The results for sample LR (non irradiated, MgO) are shown in Figures 5, 6 and 7. The extrapolated value of the penetration depth at 0 K is $\tilde{\lambda_0} = 2180 \pm 200$ Å. There is a noteworthy difference when compared to sample MA, namely the absence of a frequency dependence of $\lambda(\omega,T)$, whether analyzed in terms of a T or T^2 dependence: $c_1(\omega) \simeq 2.4 \pm 0.7$ Å K^{-1}, $c_2(\omega) \simeq 0.07 \pm 0.03$ Å K^{-2} respectively. For this sample, the experimental scatter is larger than for sample MA or MB, because less experimental runs have been performed at each frequency. The absence of a clear frequency dependence implies that the scattering rate is larger in this sample than in sample MA.

Figure 8 displays the results in sample MB (irradiated, $LaAlO_3$) for three frequencies (134, 333 and 510 GHz). We find $\tilde{\lambda_0} = 2180 \pm 200$ Å. In contrast with the two previous samples, the three curves in sample MB have entirely

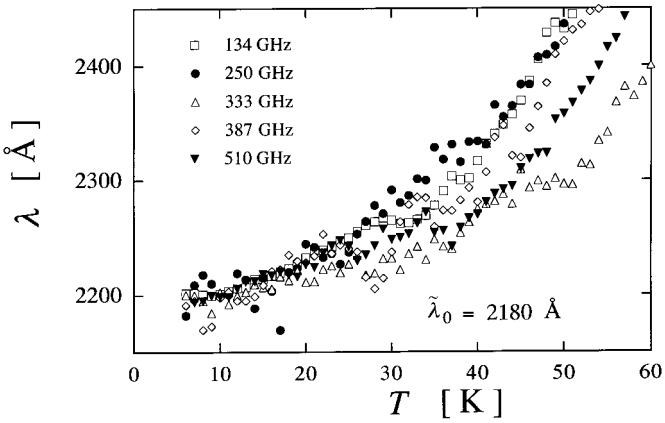

Fig. 5. Penetration depth for sample LR *versus* temperature for $T \leq 60$ K at five frequencies: 134, 250, 333, 387, 510 GHz. Above 60 K, the derivation of $\lambda(\omega,T)$ is no longer valid. $\tilde{\lambda_0}$(extrapolated) = 2180 Å. There is no frequency dependence for $T \leq 30$ K, but the curves are clearly separated from each other above ~ 40 K.

collapsed up to 40 K. The penetration depth is independent of the frequency, which again can be understood in terms of a large scattering rate ($\omega\tau \ll 1$). Moreover, the deviations for $T > 40$ K are almost negligible. Secondly, in contrast with the two other samples, the inset of Figure 8 shows a clear T^2 dependence, holding up to 40 K. $c_2(\omega) = 0.07 \pm 0.03$ Å K^{-2}.

Overall, samples MB and LR appear to bear some similarity, somewhat surprisingly given the fact that they are actually different, whereas sample MA exhibits a shorter penetration depth and a significant effect of the frequency.

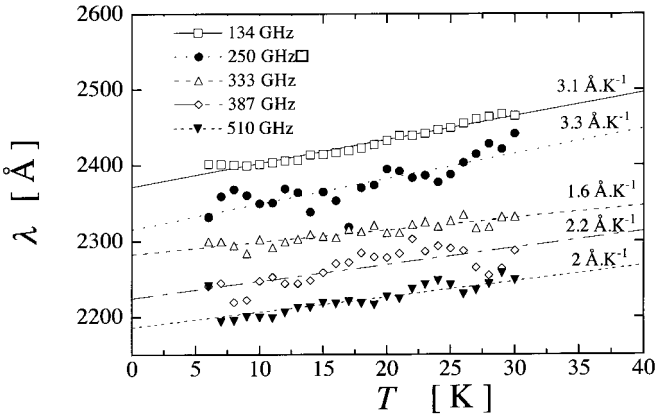

Fig. 6. Penetration depth from sample LR *versus* temperature T for $T \leq 30$ K (where a linear regime is commonly observed in single crystals) for five frequencies: 134, 250, 333, 387, 510 GHz. Best fits to a linear variation $\lambda(\omega, T) = \tilde{\lambda_0} + c_1(\omega)\, T$ are displayed for each curve as well as the value $c_1(\omega)$ of the slope. The curves are systematically shifted up by 50 Å for clarity. The average slope is 2.4 Å K^{-1}.

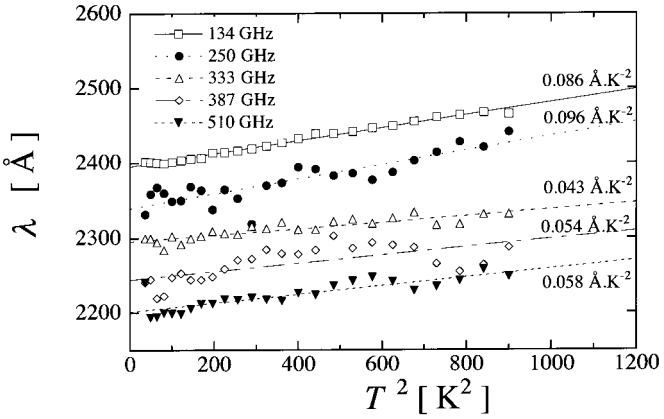

Fig. 7. Same data as in Figure 6 plotted *versus* T^2. Best fits to a T^2 variation variation $\lambda(\omega, T) = \tilde{\lambda_0} + c_2(\omega)\, T^2$ are displayed for each curve, as well as the value of $c_2(\omega)$. The average slope is 0.064 Å K^{-2}. As in sample MA, within the accuracy of the measurement, we cannot really distinguish between a T or T^2 dependence.

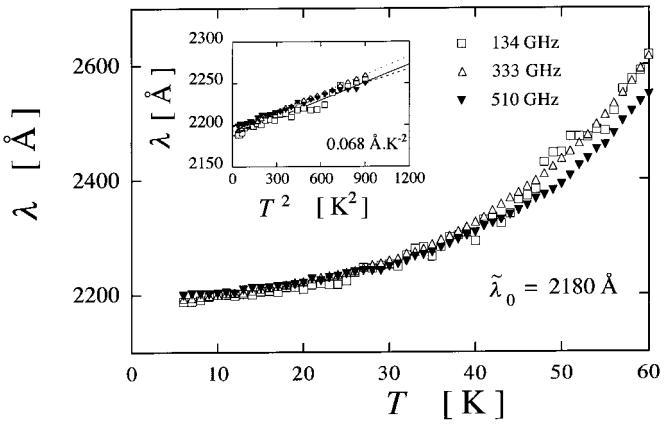

Fig. 8. Penetration depth for sample MB *versus* temperature for $T \leq 60$ K at three frequencies: 134, 333, 510 GHz. Above 60 K, the derivation of $\lambda(T)$ is no longer valid. $\tilde{\lambda_0}$(extrapolated) = 2180 Å. There is no frequency dependence for $T \leq 30$ K. The inset shows the data plotted *versus* T^2. In contrast with MA and LR, the curves collapse in a large temperature range typically up to 50 K.

6 Analysis

We now turn to a more quantitative analysis in the framework of the two fluids model, which makes use of a Drude conductivity for the normal fluid, involving a frequency independent scattering rate $1/\tau$. This model has been widely used in order to analyze the conductivity, whether in the microwave range [23,31,35,36,54] or the THz regime [37, 39]. One reason for using it is that it yields the right trends. The maximum in the real part $\sigma_1(\omega, T)$ of the conductivity below T_c, observed in single crystals [31,35, 36,54] and in thin films [24,25,37–39] can be interpreted within the two fluids model, as a result of the rapid decrease of the scattering rate $1/\tau$ below T_c. It is found experimentally that this maximum of $\sigma_1(\omega, T)$ shifts to higher temperatures, and its magnitude decreases as the frequency increases. This is understood within the same framework, where the maximum is shown to occur when $\omega\tau \sim 1$. Meanwhile, the two fluids model is also widely recognized as being inappropriate. Such a simple phenomenology does not describe properly $\sigma_1(\omega, T)$ in BCS superconductors. In high-T_c superconductors, it does not yield a quantitatively correct description of the conductivity and of the scattering rate as a function of frequency and/or temperature. From the experimental point of view, there are indeed indications that the scattering rate is frequency dependent [23,38,39]. On the theoretical side, the conductivity $\sigma_1(\omega, T)$ has been evaluated by Hirschfeld *et al.* for unconventional *d*-wave superconductors [16,17]. In the so-called pure regime and for a very small concentration of impurities, a Drude-like conductivity is recovered however the scattering rate is frequency dependent $(1/\tau(\omega))$ [16,17,24]. Under specific assumptions, $1/\tau(\omega)$ may not depend upon the frequency, but the whole calculation does not provide an actual support for the use of the standard two fluids model where $1/\tau$ depends only on temperature. Interestingly, the change of $\omega\tau$ from $\omega\tau \ll 1$ to $\omega\tau \gg 1$ yields a definite change in the temperature dependence of $\lambda(\omega, T)$ at low temperature. For the sake of the comparison with earlier data in the literature, and also in order, as mentioned above, to establish the order of magnitude for $1/\tau$ from the penetration depth data, we nevertheless perform the analysis of our data using this phenomenology. The change in the penetration depth $\lambda(\omega, T)$ with the frequency (from 100 GHz to 500 GHz) was described in an earlier paper within the assumption of a linear behavior of $\lambda(\omega, T)$ [45]. The calculation of $\lambda(\omega, T)$ used the two fluids model for three frequencies 130, 330, 510 GHz and considered various elastic scattering rates $1/\tau_{el}$, each one combining according

to Mathiessen law with the inelastic scattering rate $1/\tau_{inel}$, the latter being assumed to be adequately described by the data taken from single crystals [31,35,36]. We recall briefly how the calculation was performed when applied to $\lambda(\omega,T)$ and not to $\sigma_1(\omega,T)$ as usual: the superfluid and normal fluid fractions are $x_s(T)$ and $x_n(T)$ respectively, so that $x_s(T)+x_n(T)=1$; $x_s(T)=\tilde{\lambda_0^2}/\lambda^2(\omega=0,T)$. One assumes a Drude form for the frequency dependence of the normal fluid conductivity. Thus, the real and imaginary parts of the total conductivity write:

$$\sigma_1(\omega,T)=\frac{1}{\mu_0\omega\tilde{\lambda_0^2}}\ x_n(T)\ \frac{\omega\tau}{1+\omega^2\tau^2} \tag{5}$$

$$\sigma_2(\omega,T)=\frac{1}{\mu_0\omega\tilde{\lambda_0^2}}\left[x_n(T)\frac{\omega^2\tau^2}{1+\omega^2\tau^2}+x_s(T)\right]. \tag{6}$$

Note that equation (6) gives an explicit expression of $\lambda(\omega,T)$, which was introduced more formally in equation (3). The two extreme cases are now easily understood: for $\omega\tau\ll 1$ (quasi-static regime), the first term of $\sigma_2(\omega,T)$ is negligible at low temperatures and $\lambda(\omega,T)$ is just the frequency independent London penetration depth $\lambda_L(T)$. For $\omega\tau\gg 1$ (collisionless regime), $\lambda(\omega,T)=\tilde{\lambda_0}$ = constant, so that the penetration depth is both frequency and temperature independent, as indeed observed in the infrared range above $20\,\mathrm{cm}^{-1}$ (600 GHz) [53]. The underlying physics is that, as $\omega\tau$ increases, the inductive contribution of the normal fluid increases and yields an additional screening of the electromagnetic field, thus a smaller increase of the penetration depth with temperature, the maximum possible screening corresponding to $\tilde{\lambda_0}$. Note that this calculation cannot explain an increased penetration depth $\tilde{\lambda_0}$.

We may now come back to Table 2, which displays for sample MA the values of the parameters $c_n(\omega)$ ($n=1$ and $n=2$) where $\lambda(\omega,T)=\tilde{\lambda_0}+c_n(\omega)T^n$. Assuming a constant scattering rate at low temperatures ($T<30\,\mathrm{K}$, not inconsistent with the published results) and using (6), the two fluids model yields the frequency dependence of $c_n(\omega)$ *whatever* n:

$$c_n(\omega)=\frac{c_n(0)}{1+\omega^2\tau^2}. \tag{7}$$

Figures 9 and 10 show a fit to (7) of the experimental data from sample MA for c_n ($n=1$ and $n=2$, see Tab. 2) *versus* the frequency. Two fitting parameters are required: $c_n(0)$ and $1/\tau$. For the sake of internal consistency, the scattering rate deduced from the fit for $n=1$ and $n=2$ must be the same. We find indeed the best agreement in both cases for $1/\tau=1.7\times10^{12}\,\mathrm{s}^{-1}$. As a comparison, Bonn *et al.* [35], estimating $1/\tau$ for YBCO single crystals within the two fluids model, obtain a value of $1/\tau=5\times10^{11}\,\mathrm{s}^{-1}$, 3 times smaller than the value we find. Our result is closer to the value $1.4\times10^{12}\,\mathrm{s}^{-1}$ found for a 0.31% Zn-doped single crystal [36], where the authors show that adding Zn impurities increases the low temperature limit of the scattering rate. Therefore the scattering rate in sample MA appears to be closer to the one of a single crystal with impurities, which confirms the common idea that the films contain more defects than the single crystals. The nature of these defects remains to be identified, as they seem to affect very differently the absolute value, the temperature variation and the frequency dependence of $\lambda(\omega,T)$. We will discuss the two latter topics further.

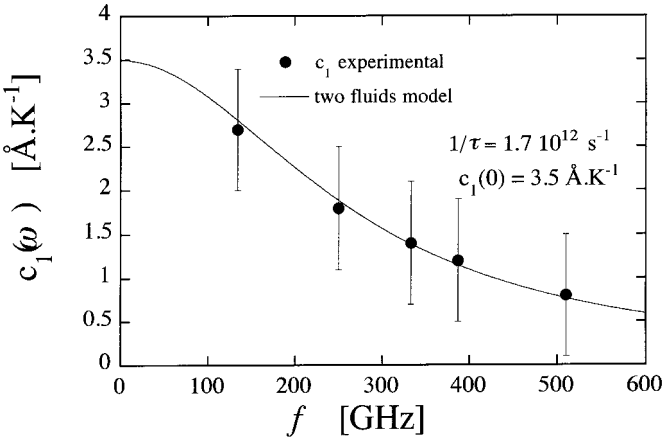

Fig. 9. Experimental data $c_1(\omega)$ from $\lambda(\omega,T)=\tilde{\lambda_0}+c_1(\omega)T$ at five frequencies from the data shown in Figure 3 along with the fitting parameters $1/\tau$ and $c_1(0)$. $1/\tau=1.7\times10^{12}\,\mathrm{s}^{-1}$. $c_1(0)=3.5\pm0.7$ Å K^{-1}, consistent with the canonical slope found in single crystals.

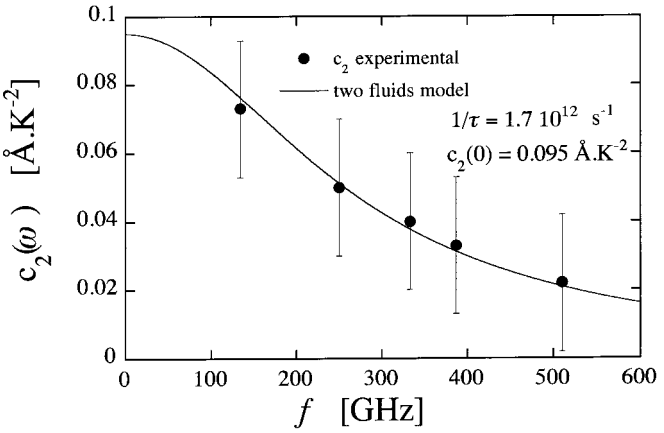

Fig. 10. Experimental data $c_2(\omega)$ from $\lambda(\omega,T)=\tilde{\lambda_0}+c_2(\omega)T^2$ at five frequencies from the data shown in Figure 4 along with the fitting parameters $1/\tau$ and $c_2(0)$. The scattering rate $1/\tau$ is the same as in Figure 9.

The second parameter we obtain from the fit is the slope at zero frequency $c_n(0)$. For $n=1$, $c_1(0)=3.5\ \pm$ 0.7 Å K^{-1}. It is compatible with the canonical value $\simeq$ 4 Å K^{-1} found in single crystals [1]. For $n=2$, $c_2(0)=$ $0.10\ \pm\ 0.03$ Å K^{-2}; we will use this in the next section.

The scattering rate for sample LR is not measurable in our experimental setup since the temperature variation of the penetration depth is not frequency dependent within

our experimental accuracy. However from a putative fit to (7) compatible with the experimental uncertainty, we can estimate a lower bound of $3 \times 10^{12}\,\mathrm{s}^{-1}$.

MB is a somewhat special sample since point defects have been introduced on purpose by irradiation. This sample was similar to sample MA before irradiation (same growth conditions, same resistivity, same T_c). The irradiation lowered T_c down to 87.8 K, and raised the 110 K resistivity to 105 $\mu\Omega$cm. The defects introduced by irradiation are thought to act as extra scattering centers. This is roughly consistent with the resistivity data. The normal state resistivity after irradiation has increased, and it is still linear with temperature; the slope is however slightly different from the one of the pristine sample, contrary to what is observed in similarly irradiated films [49] and electron irradiated crystals [55]. In order to check the consistency of our data with the condition $\omega\tau \ll 1$ expected to be fulfilled in this sample, we do the following estimate. In single crystals, above T_c, a typical 80 $\mu\Omega$cm resistivity corresponds to an inelastic scattering rate $1/\tau_{inel} = 3 \times 10^{13}\,\mathrm{s}^{-1}$ [31]. The increase of resistivity at 110 K introduced by irradiation is then equivalent to adding $1/\tau_{el} \simeq 9 \times 10^{12}\,\mathrm{s}^{-1}$. A calculation in the two fluids framework shows indeed that taking $1/\tau_{el} \simeq 10^{13}\,\mathrm{s}^{-1}$ yields no frequency dependence in $\lambda(\omega, T)$ within our experimental resolution. This also explains qualitatively why the penetration depth in sample MB hardly shows any frequency dependence even for $T > 40$ K (Fig. 8).

We have shown in this section that the two fluids model allows a reasonable understanding of the experimental data if not yielding the exact figures. The underlying physics in (7), whose simplicity derives of course directly from the two fluids model, is that the measuring frequency is comparable to the scattering rate. Whichever specific model we may use, we expect that when these two figures are of the same order of magnitude, the experimentally measured penetration depth must be modified, which is indeed what is derived in [16,17].

7 Discussion of the d-wave model and the resonant scattering

None of our samples exhibit an optimal $T_{c0} = 92$ K. Our penetration depth data are not accurate enough so as to make a clear distinction between a T or T^2 dependence at $T \leq 30$ K. In this temperature range, the temperature dependence for $\lambda(\omega = 0, T)$ in sample MA is consistent with the standard linear behavior (~ 4 Å K^{-1}). The two other samples exhibit a slower increase of $\lambda(\omega = 0, T)$ with temperature: this appears when comparing for instance the increase of $\lambda(\omega = 0, T)$ which is characterized in the first column of Table 3 by the parameter $c_2(0)$.

All the samples display a penetration depth $\tilde{\lambda_0}$ significantly increased with respect to the generally accepted value $\lambda_0 = 1400 \pm 100$ Å [52,53]. In this section, we analyze the data in the framework of the d-wave model with impurity scattering, somewhat similarly to what was done in single crystals and thin films [24,27,31,32]. The noticeable difference with earlier work is that we may now use a reliable and more accurate measurement of $\tilde{\lambda_0}$ to estimate the change $\delta\lambda_0 = \tilde{\lambda_0} - \lambda_0$. We proceed as follows: $\delta\lambda_0$ is related to the parameter $c_2(0)$ which controls the variation of the penetration depth in the gapless regime [15–17]. From $c_2(0)$, we deduce the cross-over temperature where the linear regime is recovered, T^*, using $\lambda_0 = 1400$ Å and $\Delta_0 = \lambda_0 \ln 2/c_1(0) = 243\,K$ (from the standard value $c_1(0) = 4$ Å K^{-1} in crystals). This yields the expected change $\delta\lambda_0$–theoretical in the framework of the model, assuming the unitary limit, which we compare to our estimate $\delta\lambda_0$–experimental. The values of $c_2(0)$, T^*, $\delta\lambda_0$–theo and $\delta\lambda_0$–exp are displayed in the first four columns of Table 3 where it can be seen that $\delta\lambda_0$–exp is about three times larger than expected from $c_2(0)$. Earlier work skipped the estimate of T^* by plotting $\delta\lambda_0$ *versus* $c_2(0)$, or a similar parameter association. It is instructive though to quote T^* (directly related to the scattering rate, hence the impurity concentration) which is anomalously large: one would expect $T^* < 30$ K, since the model predicts that the linear regime is recovered above T^*, and in YBCO, this linear regime only holds up to 30 K. This may point one possible reason why the model does not work, before ruling it out, namely the amount of impurities or defects in the films is too large and the model does no longer apply. We also deduce from the model [14] the reduction of T_c (T_c/T_{c0}–theo) associated to $\delta\lambda_0$–exp (shown in the last two columns of Tab. 3) and we compare it to the actual ratio, (T_c/T_{c0}–exp). Again, this comparison shows that even in the unitary limit, the experimental increase of λ_0 should be associated with a larger decrease of the critical temperature. This confirm the failure of the model to account for the decrease of the critical temperature related to the decrease of the superfluid density, hence the increase of λ_0. Therefore, although it is commonly quoted that the films may bear some similarity with the impurity doped single crystals, our data compared with the theoretical expectations in the d-wave model show that this similarity is far from being obvious, once the absolute value of $\tilde{\lambda_0}$ is determined.

Table 3. Comparison of the experimental $\delta\lambda_0$–exp and theoretical $\delta\lambda_0$–theo, changes of the penetration depth deduced from the c_2 parameter [15]. T^* is the cross-over temperature, also deduced from c_2. The Table shows also the experimental and theoretical relative change of the critical temperature (T_c/T_{c0}) expected from $\delta\lambda_0$–exp, in the framework of the d-wave model with impurity scattering [14] (see text).

	c_2 (Å K^{-2})	T^* (K)	$\delta\lambda_0$ theo (Å)	$\delta\lambda_0$ exp (Å)	T_c/T_{c0} theo	T_c/T_{c0} exp
MA	0.095	42	195	590	0.75	0.98
LR	0.07	60	254	780	0.6	0.95
MB	0.07	59	252	780	0.6	0.96

Our discussion is of course only valid if we assign the increase of the penetration depth with respect to the intrinsic value entirely to resonant scattering due

to impurities. It is however quite possible that this increase may be related to other very different defects. To illustrate this point, we discuss briefly the example of extended defects such as grain boundaries, likely to be present in thin films. Grain boundaries which form resistively shunted Josephson junctions with Josephson penetration depth λ_J lead to an effective penetration depth λ_{eff} which reads [56]: $\lambda_{eff}^2 = \tilde{\lambda_0^2} + \lambda_J^2$. The effect of the grain boundaries is then to enhance the intrinsic penetration depth, which would provide an explanation for the large values that we find. A first question which arises immediately is whether such grain boundaries may be effective for scattering. Recall indeed that we find evidence for a scattering rate $1/\tau = 1.7\times10^{12}\,\mathrm{s}^{-1}$ in sample MA, which suggests a good quality, in contrast with the large penetration depth. With a Fermi velocity $v_F = 2 \times 10^7\,\mathrm{cms}^{-1}$ [57], the QP mean free path ℓ at low temperature would be $\ell = v_F\tau = 1300$ Å, which is roughly the size of the grains [58]. Hence grain boundaries may be weakly scattering, which does not contradict their being responsible for a large penetration depth. This assumption does not however look acceptable since all the films under investigation exhibit standard critical current densities, which imply firstly presumably a short λ_J, secondly an extra temperature variation due to λ_J. Indeed, the Josephson critical current in an unconventional superconductor with nodes in the gap is expected to display a definite temperature dependence at low temperature (unlike the standard BCS Ambegaokar-Baratoff expression) [59]. This yields a more complicated temperature dependence for λ_{eff}, which must be difficult to identify.

Another explanation could be the occurrence of pinholes in the films. However, putting numbers rules out such a possibility: a typical amount of pinholes would give rise at most to 10% leakage [60]. Such a leakage results in an increase of ~ 50 Å for the penetration depth, and we are looking for an increase of ~ 500 Å (see $\delta\lambda_0$– experimental in Tab. 3).

8 Conclusion

We have established in a pristine sample $YBCO/LaAlO_3$, a definite effect of the frequency on the measured penetration depth, *e.g.* the low temperature variation gets smaller as the frequency increases (a similar effect has been observed in two other samples from a different origin). The discussion of the actual temperature dependence of the penetration depth $\lambda(\omega, T)$ has been purposely skipped here and is postponed to a further report. The frequency effect can be consistently described by the two fluids model, which yields the low temperature scattering rate. However, this two fluid analysis has so far no reliable theoretical background for unconventional superconductors. We have stressed that the evolution of this temperature dependence with frequency results more generally from a competition between the scattering rate and the frequency. In this respect, our experiment puts a reasonable order of magnitude for the quasi-particle scattering time in thin films at low temperature.

Our comparison to the *d*-wave model shows that this model fails to account for the various parameters which are measured and which are expected to be related through the theory. We note that this failure does not necessarily rule out the validity of the model. Indeed, our final discussion raises several caveat: firstly, although our samples look as good if not better than the ones referred to in the literature, they may still include too many defects, which then puts them out of the range of validity of the model. Secondly, although we insist on the essential knowledge of $\tilde{\lambda_0}$, an increased penetration depth may result from extrinsic sources yet to be identified, in which case its value cannot be taken for the comparison with the theory. Therefore the major point which we eventually wish to strongly emphasize is that any comparison with a theoretical model, should be considered with extreme care. Even in experimentally satisfactory conditions, where a fairly complete set of parameters is available, such a comparison may be still ambiguous.

We are very grateful to G. Deutscher and P. Monod for many illuminating discussions and helpful suggestions.

References

1. W.N. Hardy *et al.*, Phys. Rev. Lett. **70**, 3999 (1993).
2. T. Jacobs *et al.*, Phys. Rev. Lett. **75**, 4516 (1995).
3. S.F. Lee *et al.*, Phys. Rev. Lett. **77**, 735 (1996).
4. D.M. Broun *et al.*, Physica C **282-287**, 1467 (1997).
5. C. Panagopoulos *et al.*, Phys. Rev. B **53**, R2999 (1996).
6. H. Ding *et al.*, Phys. Rev. Lett. **74**, 2784 (1995).
7. K.A. Koutnetzov *et al.*, Phys. Rev. Lett. **79**, 3050 (1997).
8. K. Maki, M.T. Beal-Monod, Phys. Lett. A **208**, 365 (1995).
9. J. Bouvier, J. Bok, Physica C **249**, 117 (1995).
10. N.S. Achaf *et al.*, Physica C **282-287**, 140 (1997).
11. H. Srikanth *et al.*, Phys. Rev. B **55**, R14733 (1997).
12. P. Monthoux, D. Pines, Phys. Rev B **47**, 6069 (1993).
13. R. Combescot, X. Leyronas, Phys. Rev. Lett. **75**, 3732 (1995).
14. H. Kim, G. Preosti, P. Muzikar, Phys. Rev. B **49**, 3544 (1994).
15. P.J. Hirschfeld, N. Goldenfeld, Phys. Rev. B **48**, 4219 (1993).
16. P.J. Hirschfeld, W.O. Putikka, D.J. Scalapino, Phys. Rev. Lett. **71**, 3705 (1993).
17. P.J. Hirschfeld, W.O. Putikka, D.J. Scalapino, Phys. Rev. B **50**, 10250 (1994).
18. D.A. Bonn, W.N. Hardy, in *Physical Properties of High Temperature Superconductors V*, edited by D.M. Ginsberg (World Scientific, Singapore, 1995), p. 7.
19. J. Mao *et al.*, Phys. Rev. B **51**, 3316 (1995).
20. L.A. de Vaulchier *et al.*, Europhys. Lett. **33**, 153 (1996).
21. O.M. Froelich *et al.*, Phys. Rev. B **50**, 13894 (1994).
22. T.R. Lemberger, E.R. Ulm, K.M. Paget, V.C. Matijasevic, Oxide Superconductor Physics and Nanoengineering II, 1996.
23. T. Shibauchi *et al.*, J. Phys. Soc. Jpn **65**, 3266 (1996).

24. S. Hensen, G. Müller, C.T. Rieck, K. Sharnberg, Phys. Rev. B **56**, 6237 (1997).
25. E. Farber, G. Deutscher, J.P. Contour, E. Jerby, preprint.
26. J. Annett, N. Goldenfeld, S.R. Renn, Phys. Rev. B **43**, 2778 (1991).
27. Z. Ma *et al.*, Phys. Rev. Lett. **71**, 781 (1993).
28. J.Y. Lee *et al.*, Phys. Rev. B **50**, 3337 (1994).
29. H.E. Porteanu *et al.*, Phys. Rev. Lett. **75**, 3934 (1995).
30. B.J. Feenstra *et al.*, Physica C **278**, 213 (1997).
31. D.A. Bonn *et al.*, Phys. Rev. B **40**, 4051 (1994).
32. E.R. Ulm *et al.*, Phys. Rev. B **51**, 9193 (1995).
33. L.A. de Vaulchier, Ph.D. thesis, Paris VI University, 1995.
34. R.C. Budhani *et al.*, Phys. Rev. B **44**, 7087 (1991).
35. D.A. Bonn *et al.*, J. Phys. Chem. Solids **54**, 1297 (1993).
36. D.A. Bonn *et al.*, Phys. Rev. B, 11314 (1993).
37. U. Dähne *et al.*, J. Supercond. **8**, 129 (1995).
38. M.C. Nuss *et al.*, Phys. Rev. Lett. **66**, 3305 (1991).
39. A. Frenkel *et al.*, Phys. Rev. B **54**, 1355 (1996).
40. L.A. de Vaulchier *et al.*, Phys. Rev. B **52**, 564 (1995).
41. R.E. Glover, M. Tinkham, Phys. Rev. **108**, 243 (1957).
42. M. Tinkham, *Introduction to superconductivity*, 1975.
43. G. Preosti, H. Kim, P. Muzikar, Phys. Rev. B **50**, 1259 (1994).
44. M.R. Beasley, Physica C **185-189**, 227 (1991).
45. N. Bontemps, L.A. de Vaulchier, R. Combescot, Ferroelectrics **177**, 127 (1996).
46. A.A. Volkov, N. Klein, Infrared Phys. **25**, 369 (1985).
47. R.P.S.M. Lobo, private communication.
48. P. Roy *et al.*, private communication.
49. A.W. Connell *et al.*, Physica C **225**, 7 (1994).
50. C.L. Paven-Thivet *et al.*, Physica C **244**, 231 (1995).
51. X. Castel *et al.*, Physica C **255**, 281 (1995).
52. J.E. Sonier *et al.*, Phys. Rev. Lett. **72**, 744 (1994).
53. D.N. Basov *et al.*, Phys. Rev. Lett. **74**, 598 (1995).
54. T. Shibauchi *et al.*, Physica C **203**, 315 (1992).
55. J. Giapintsakis, D.M. Ginsberg, M.A. Kirk, S. Ockers, Phys. Rev. B **50**, 15967 (1994).
56. T.L. Hylton *et al.*, Appl. Phys. Lett. **53**, 1343 (1988).
57. P.B. Allen *et al.*, Phys. Rev. B **37**, 7482 (1988).
58. A. Perrin, private communication.
59. H. Burkhardt *et al.*, preprint.
60. S. Moffat, private communication.